The International Journal of Advanced Manufacturing Technology (2019) 102:1703–1717
https://doi.org/10.1007/s00170-019-03287-z

ORIGINAL ARTICLE

Modeling and optimization of Wire-EDM parameters for machining of $Ni_{55.8}Ti$ shape memory alloy using hybrid approach of Taguchi and NSGA-II

Raymond Magabe[1] · Neeraj Sharma[1] · Kapil Gupta[1] · J Paulo Davim[2]

Received: 12 October 2018 / Accepted: 2 January 2019 / Published online: 11 January 2019

Abstract
In the present research, $Ni_{55.8}Ti$ shape memory alloy has been machined by wire electric discharge machining (wire-EDM) process. The effects of input parameters such as spark gap voltage, pulse on-time, pulse off-time, and wire feed on productivity, i.e., metal removal rate (MRR) and surface quality, i.e., mean roughness depth (R_z), have been investigated. Empirical modeling and ANOVA study have been done after conducting 16 experiments based on Taguchi's L_{16} design of experiment technique. Ranking and crowding distance–based non-dominated sorting algorithm-II (NSGA-II) is used for process optimization. The error percentage varies within ± 6% between experimental results and the predicted results developed by NSGA-II. It has been observed that the wire-EDM machining of $Ni_{55.8}Ti$ alloy at optimum parameters resulted in improved MRR —0.021 g/min— and surface quality with good surface finish (R_z—6.2 μm) and integrity as significant reduction in the formation of cracks, lumps, and deposited layers.

Keywords Biomedical · NiTi · NSGA-II · Optimization · Surface integrity · Wire-EDM

1 Introduction

Shape memory alloys are "smart" materials that can change their form (shape or size) and can return back to their original form with applied heat, stress, or magnetic field. They have the ability to produce very high actuation strain, stress, and work output due to reversible martensitic phase transformations [1–3]. These alloys are compact, robust, lightweight, frictionless, quiet, biocompatible, environmentally friendly, and possess superior properties in actuation, vibration damping, and sensing. Since their discovery in 1932 to now, there has been extensive development in the field and many types of alloys are commercially available for various applications. Nickel titanium (NiTi)-based shape memory alloys find extensive applications in biomedical and engineering fields due to their higher corrosion and wear resistance, and superior thermal stability and biocompatibility compared to other shape memory alloys. The material titanium present in the NiTi alloy makes a protective layer (TiO_2) and prevents the release of Ni ions into the biofluid which makes this material suitable for biomedical implants. The applications of $Ni_{55.8}Ti$ are found in biomedical field (especially in orthodontics) where it is used preferably over stainless steel and Co-Cu alloy [1, 4].

The machining of shape memory alloys by conventional processes is difficult due to their high ductility, typical stress-strain behavior, low thermal conductivity, and high degree of work hardening [2, 5]. It results excessive tool wear, burr formation, poor work surface integrity, very high consumption of energy and resources, escalated cost of fabrication and processing, and high environmental footprints.

This compels to explore advanced processes for machining of shape memory alloys. Biomedical applications require complex shape implants and structures made of $Ni_{55.8}Ti$ alloys. Wire-EDM or WEDM is a well-known advanced machining process to fabricate complex shapes and features in difficult-to-machine materials [6, 7]. Therefore, wire-EDM

✉ Kapil Gupta
kgupta@uj.ac.za

[1] Department of Mechanical and Industrial Engineering Technology, University of Johannesburg, Doornfontein Campus, 7225-John Orr Building, Doornfontein, 2028 Johannesburg, Republic of South Africa

[2] Department of Mechanical Engineering, University of Aveiro, Aveiro, Portugal

has been selected to machine $Ni_{55.8}Ti$ alloy in the present work to achieve good machinability.

Wire-EDM works on the principle of thermo-electric erosion that is achieved by generation of spark between workpiece (as anode) and wire electrode (as cathode) under the influence of suitable dielectric fluid [8]. Figure 1 presents the working principle of wire-EDM process. Some of the most important WEDM parameters which influence the work surface quality, cutting rate, and material removal rate are pulse-on time, pulse-off time, servo voltage, current, and wire speed.

There has been some past work conducted on wire-EDM of shape memory alloys. Some of the important results of recent investigations are discussed here as under.

Manjaiah et al. [9, 10] conducted a detailed investigation on WEDM of different grades of NiTi material. Increasing material removal rate with pulse-on and improving surface roughness characteristics with pulse-off time have been found. High discharge energy and intensity of spark at long pulse-on time and adequate flushing in the machining zone due to longer pulse-off time are the reasons behind that. Later, desirability-based multi-performance optimization secured optimal WEDM parameters for the best machinability of SMA with 1.83-μm average roughness and 7.6 mm/min material removal rate. Furthermore, the XRD study informed the presence of thermal damage as the formation of oxide and other phases took place corresponding to longer pulse-on time [9]. Low pulse-on time with high voltage has been recommended for enhanced surface quality. Another investigation also reports almost same trends and additionally with higher hardness along longer pulse-on time due to high discharge melting and rapid solidification of molten material that probably increased the carbide content percentage on the machined surface of SMA. Interaction between pulse-on time and voltage has been identified as one of the most important factors to be considered in WEDM of SMAs. SMA machining with coated brass wire resulted in lower MRR compared to plain brass wire [10]. Interestingly, machining with increased wire speed caused higher material removal rate as the molten material is splashed around the surface by flushing pressure and discharge of large gas volume from the molten pool increases material removal rate [10]. Sharma et al. [11] machined the porous $Ni_{40}Ti_{60}$ by WEDM at different parameter settings. The minimum to maximum variations of cutting speed, surface roughness, and dimensional deviation are 0.11 to 1.97 mm/min, 1.33–5.75 μm, and 0.0519 to 0.1397 mm, respectively. Soni et al. [12] conducted an experimental research to study the influence of WEDM parameters on surface integrity of $Ti_{50}Ni_{40}CO_{10}$ alloy. They observed increment in MRR and surface roughness with high pulse-on time and low pulse-off time, while increase in servo voltage decreased their values. Machining at pulse-on time above 125 μs and voltage below 20 V deteriorated surface morphology and led to the formation of a very thick recast layer. Conclusively, wire-EDM of $Ti_{50}Ni_{40}CO_{10}$ alloy at low pulse of time and high voltage has been recommended for better results. Bisaria and Shandilya [13] studied the effect of WEDM parameters on cutting efficiency, micro-hardness, and surface roughness R_a during machining of $Ni_{50.89}Ti_{49.11}$. They found spark off-time, spark on-time, and servo voltage as the significant parameters. It was observed that the micro-hardness on the machined surface was many times the hardness of the starting material due to the formation of recast layer of thickness 20–35 μm. Moreover, various oxides and chemical compounds such as Cu_5Zn_8, Cu_4O_3, and TiO have been formed on the machined surface after WEDM.

After a detailed review of the available literature, it is found that a minute change in the composition of NiTi shape memory alloy may change its characteristics and post-machining properties. Moreover, there is a scarcity of work on wire-EDM of $Ni_{55.8}Ti$ alloy, and in previous work, mean roughness depth which gives the clear indication of machined surface roughness has not been considered.

The aforementioned gap is fulfilled in the present work where wire-EDM of $Ni_{55.8}Ti$ alloy has been done. Two important machinability indicators, i.e., material removal rate (MRR) that depicts process productivity and mean roughness depth that indicates surface quality, are evaluated in the present work, and the effects of wire-EDM parameters are analyzed on these machinability indicators. Regression analysis and ANOVA study have been done to find the significant wire-EDM parameters. Empirical modeling has been done to establish the relationship between wire-EDM parameters and machinability indicators. Non-dominated sorting genetic algorithm (NSGA) II–based optimization of wire-EDM process has been done to secure optimum values of wire-EDM parameters for the best values of MRR and mean roughness depth. The results have been accompanied by SEM investigation to study the morphology of $Ni_{55.8}Ti$ alloy surface after wire-EDM.

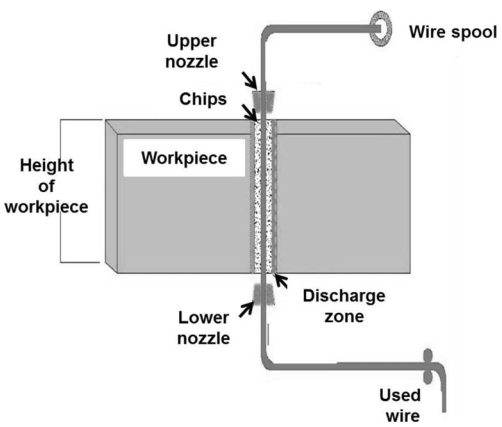

Fig. 1 Schematic representation of working principle of wire-EDM

2 Experimentation and measurement

In the present work, $Ni_{55.8}Ti$ specimens of 2.5-mm thickness each have been machined from a bar of 16-mm diameter and 200-mm length. The as-received NiTi SMA has 885 MPa tensile strength, 6.45 g/cm^3 density, and 333 HV micro-indentation hardness. Figure 2 presents the composition of shape memory alloy used in the present work. As seen in Fig. 2, it consists of 55.8% nickel, 43.9% titanium, and 0.3% carbon.

A total of 16 experiments have been conducted based on Taguchi's robust design of experiment technique where L_{16} orthogonal array has been used to derive experimental combinations. Figure 3 presents various tasks performed during wire-EDM of $Ni_{55.8}Ti$ shape memory alloys.

The specimens have been machined on Electronica make Ecocut (Elplus 15) computer numeric control (CNC) wire electric discharge machine (wire-EDM) using commercially used zinc-coated brass wire with 0.25-mm diameter and 900 MPa tensile strength as tool electrode under the influence of deionized water as dielectric. There was a wide range of input machining parameters available with the wire-EDM machine tool. The selected ranges and four levels of machining parameters such as spark gap voltage (SV), pulse on-time (P_{on}), pulse off-time (P_{off}), and wire feed (m/min) are based on literature review, machine constraints, and preliminary experiments. Table 1 presents the levels and values of variable and fixed input parameters used in the present work.

Material removal rate (MRR) is the material removed per unit of time during machining of SMA, and it was measured in grams per minute using Eq. (1) as given below:

$$\mathrm{MRR} = \frac{\text{mass of specimen before machining} - \text{mass of specimen after machining}}{\text{time taken for machining}} \quad (1)$$

Mass of specimen before and after machining is measured by Shimadzu make precise weighing balance with 0.01 mg least count. A stop watch is used to measure the machining time. TMTech Instrument make surface roughness (TMR200) tester is used to measure surface roughness, and the average of five values was considered as final result. For measurement, the cutoff and evaluation lengths are 0.8 mm and 4.0 mm, respectively. The average and maximum roughness are the two important parameters to evaluate surface quality, but the mean roughness depth R_z is the most prominent and reliable parameter that gives meaningful and the most appropriate information about the surface quality [14, 15]. The mean roughness depth is the average of maximum peak to valley of five consecutive sampling lengths within the measuring length. Therefore, mean roughness depth R_z has been used to evaluate the surface quality in the present research. The micro-structure of machined surface is evaluated using scanning electron microscopy (SEM) of Tescan make scanning electron microscope. The voltage during the SEM was kept at 20 kV. Before SEM, the surface was prepared for micro-structural study. The machined surface was prepared using different SiC papers (320, 800, 1200, 2400 grit size), starting from the courser side to finer side. After grinding with SiC papers, the samples were cleaned using acetone to remove dust particle. The cleaned samples were polished using 3-μm Al_2O_3 paste on polishing machine. The etching of

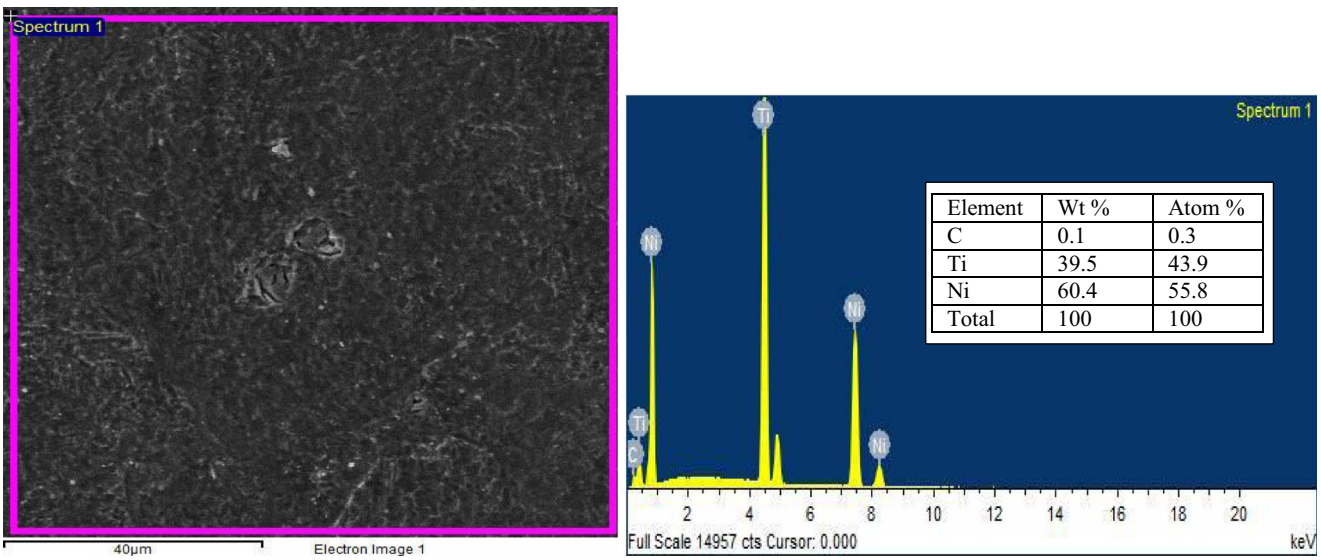

Element	Wt %	Atom %
C	0.1	0.3
Ti	39.5	43.9
Ni	60.4	55.8
Total	100	100

Fig. 2 Elemental composition of $Ni_{55.8}Ti$ using EDS

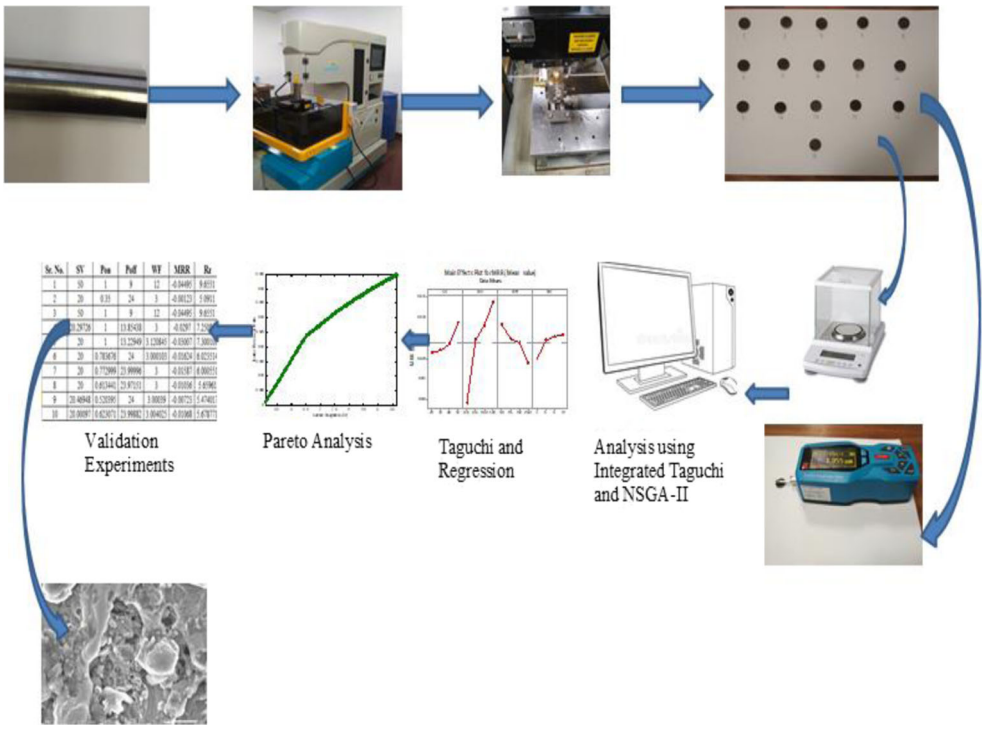

Fig. 3 Sequence of tasks performed during wire-EDM of $Ni_{55.8}Ti$ shape memory alloy

polished samples was done in a mixture of HF, HNO_3, and H_2O in the proportion of 10%, 40%, and 50%, respectively.

3 Results and discussion

Table 2 shows the 16 experimental combinations and corresponding values of MRR and R_z obtained after experimentation. For each experiment, three readings were recorded, and their mean is used for the analysis purpose. ANOVA is used for the investigations of the significant and non-significant process parameters, the percentage contribution of each process parameter affecting the responses, standard deviation, and the percentage of outcomes that are close to the fitted regression line.

The percentage contribution of each individual parameter was calculated by using SS as from Eq. (2).

$$\text{Percentage contribution} = \frac{S_i}{S_t} \times 100 \tag{2}$$

Table 1 Wire-EDM process parameters used in the present work

Variable process parameters						
Sl no.	Process parameter	Unit	Level 1	Level 2	Level 3	Level 4
1	Spark gap voltage "SV"	V	20	30	40	50
2	Pulse-on time "P_{on}"	μs	0.35	0.55	0.8	1
3	Pulse-off time "P_{off}"	μs	9	11.5	15	24
4	Wire feed rate "WF"	m/min	3	6	9	12
		Fixed process parameters				
1	Workpiece		$Ni_{55.8}Ti$ SMA			
2	Electrode		Zinc-coated brass wire (0.25-mm diameter)			
3	Dielectric		Deionized water			
7	Dielectric temperature		20–24 °C			
5	Working temperature		25 °C			
6	Wire tension		11.8 N			
7	Dielectric pressure		7 kg/cm^2			

Table 2 Experimental design matrix and results

Sr. no.	SV	P_{on}	P_{off}	WF	MRR (g/min)	R_z (μm)
1	20	0.35	9	3	0.007	6.13
2	20	0.55	11.5	6	0.024	6.73
3	20	0.8	15	9	0.026	7.54
4	20	1	24	12	0.027	7.26
5	30	0.35	11.5	9	0.009	7.13
6	30	0.55	9	12	0.028	8.16
7	30	0.8	24	3	0.017	6.40
8	30	1	15	6	0.032	8.14
9	40	0.35	15	12	0.011	7.59
10	40	0.55	24	9	0.021	6.91
11	40	0.8	9	6	0.032	7.30
12	40	1	11.5	3	0.029	8.26
13	50	0.35	24	6	0.009	6.37
14	50	0.55	15	3	0.025	7.45
15	50	0.8	11.5	12	0.036	8.76
16	50	1	9	9	0.044	9.70

where S_i is SS of individual process parameters and S_t is total SS.

For example, S_i for SV is 0.000132 and S_t is 0.001722. Therefore, using Eq. (2), the percentage contribution of SV is calculated. The F values and P values are used to identify significance of parameters [16]. The larger the F value, the higher will be the contribution of the process parameter for particular response, and reverse is true for P values. So, the smaller the P value, the larger will be the contribution of parameter. In this way, F values and P values are inversely proportional to each other. Also, the P value must be less than 0.05 to keep a process parameter significant for 95% confidence interval. Table 3 shows that all values are less than 0.05; therefore, all wire-EDM parameters significantly affect MRR. The standard deviation in this work is 0.001023 that shows that the maximum variation of MRR from the mean value is equal to the 0.001023. The value of R signifies our data fitness in the model for significant and non-significant parameters. It is also termed as coefficient of determination. Therefore, 99.8% future outcomes of the model can be predicted by the use of present data. Adjusted R is alike R with a difference that it shows future outcome or fitted regression due to significant terms only. Table 4 gives the MRR value corresponding to the particular level of a process parameter along with the rank of parameter and the difference between maximum and minimum value of MRR for a particular process parameter.

Table 3 ANOVA for means (MRR)

Parameters	DF	SS	p (%)	MS	F value	P value
SV	3	0.000132	7.65	0.000044	41.97	0.006
P_{on}	3	0.001318	76.53	0.000439	419.38	0.000
P_{off}	3	0.000184	10.68	0.000061	58.53	0.004
WF	3	0.000086	4.98	0.000029	27.40	0.011
Residual error	3	0.000003	0.16	0.000001		
Total	15	0.001722				

$S = 0.001023$; $R = 99.8\%$; adjusted $R = 99.1\%$

DF degree of freedom, *SS* sum of square, *p* percentage contribution, *MS* mean square, *P* value probability value

Figure 4 shows that the MRR increases with SV. The reason behind this is the increase in discharge energy per unit of spark due to high amount of ionization of the deionized water. So, for a specific duration of time, the number of spark remains the same while the intensity of discharge energy for each spark increases [17]. This increases the erosion rate of material and finally increases the MRR. The main mechanism of material removal from the workpiece is the conversion of discharge energy into thermal energy and thereby melting and vaporization of material. The higher the discharge energy, the higher will be the thermal energy. The discharge energy can be calculated by Eq. (3).

$$\text{Discharge Energy (DE)} = \int_0^{t_e} V_e(t) \times i_e(t) \times dt \cong V_e I_e t_e \tag{3}$$

V_e is the discharge voltage; I_e is the discharge current; t_e is the discharge time.

The value of discharge voltage in WEDM varies from 15 to 30 V, while in the present work, its value is equal to 28 V. The value of I_e in this research work is kept at 12 A. The delay time in zero ignition is equal to zero, so the discharge time (t_e) in the present work becomes equal to the pulse-on time. Mostly, the value of V_e is kept constant (28 V), but in this work, the value of I_e is also kept constant. Hence, the discharge energy totally depends upon the P_{on} value in the present case. Equation (3) after incorporating values converts to Eq. (4) as below:

$$\text{DE} = 28 \times 12 \times P_{on} \tag{4}$$

So, higher P_{on} value increases the discharge energy in the circuit. This discharge energy is the main source of thermal energy which removes the material in the form of debris. The

Table 4 Response table for means

Level	SV	P_{on}	P_{off}	WF
1	0.021	0.009	0.028	0.020
2	0.022	0.024	0.024	0.024
3	0.023	0.028	0.023	0.0255
4	0.028	0.033	0.018	0.0259
Delta	0.007	0.024	0.009	0.005
Rank	3	1	2	4

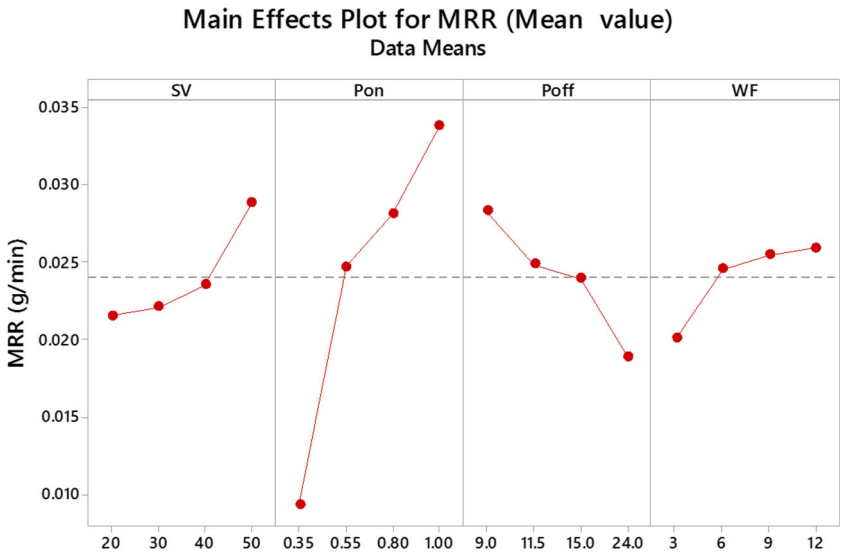

Fig. 4 Variation of MRR with the input parameters

amount and intensity of discharge energy both are increased with increase in P_{on}. Therefore, high material removal rate is achieved.

P_{off} is the time interval for deionization of dielectric and removed material to be expelled out from the machining zone [17]. For higher pulse-off duration, the number of active sparks decreases, which are responsible for discharge energy and hence reduces the MRR. So, as the P_{off} value increases, the MRR decreases, because of reduction in spark and hence amount and intensity of discharge energy.

Wire feed rate WF is the rate by which a new wire comes into play to remove the material. At low value of WF, already used wire with low machining abilities remains in the machining zone for a longer period and hence low MRR. But, at high value of WF, a fresh wire (with high cutting abilities) comes in contact with the workpiece that removes the material at a faster pace. Therefore, increase in WF increases MRR.

Contour plots where different colors are used for different range of response are used for the prediction of the effect of two factors simultaneously on a single response. Figure 5 shows the effect of P_{on} and P_{off} on MRR. The range of response according to color coding is also depicted in Fig. 5. At low value of P_{on} (i.e., up to 0.45 μs) and all P_{off} values (from 9 to 24 μs), the MRR range varies from 0.015 to 0.02 g/min. Low value of P_{off} and high value of P_{on} reveal the maximum MRR. The reason of high MRR during the high P_{on} and low P_{off} has already been explained in the previous text. This is due to high amount of discharge energy in the circuit at high P_{on} and low P_{off} for that cycle duration.

Figure 6 shows combined effect of P_{on} and SV on MRR. It has been observed from Fig. 6 that MRR varies from 0.015 to 0.020 g/min, when the P_{on} increases from 0.4 to 0.5 μs and 0.7 to 0.85 μs. Both of these MRR ranges only are found at selected values of SV. If P_{on} kept constant in between 0.7 to 0.85 μs, but SV is increased from 32 V, then the range of

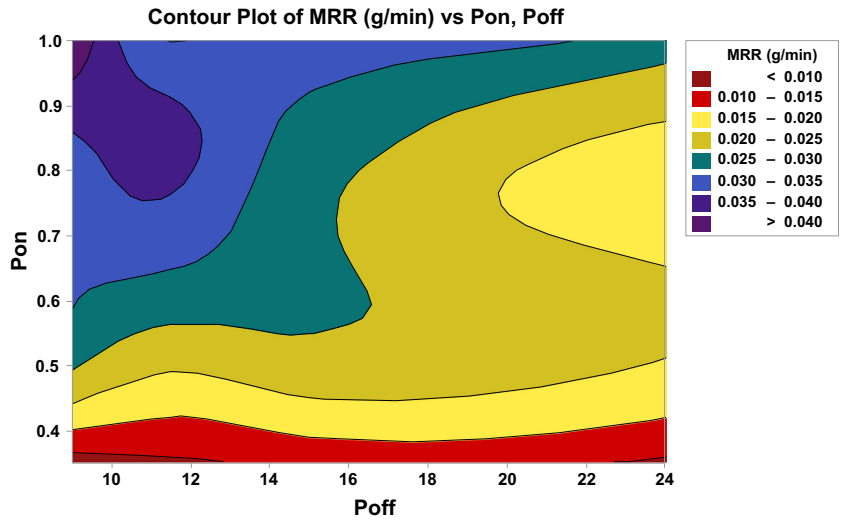

Fig. 5 Contour plot of P_{on}, P_{off}, and MRR

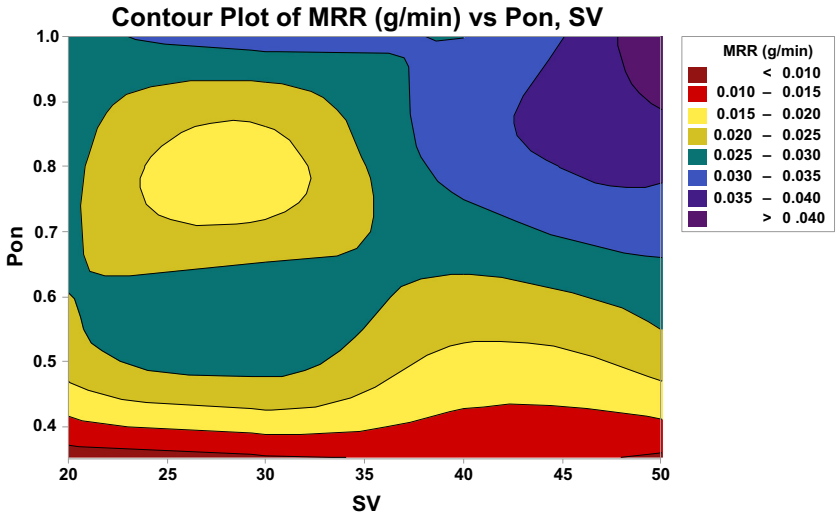

Fig. 6 Contour plot of P_{on}, SV, and MRR

MRR is 0.02 to 0.025 g/min. Similarly, keeping P_{on} within the same range and further varies SV, the MRR increased up to 0.04 g/min by observing the color coding of contour plots. The reason of increase in MRR with SV has also been clarified in the previous text.

Table 5 provides the statistical analysis for the mean values of R_z. This analysis gives the DF, SS, and percentage contribution, MS, F values, and P values for the process parameters. From the analysis, it is evident that all the P values are below 0.05, so all the process parameters are significant and play a major role in the variation of R_z. The percentage contribution in the R_z is computed using Eq. (2).

It is evident from Fig. 7 that the major contributing factor for R_z is P_{on} followed by P_{off}, SV, and WF. The standard deviation for R_z is 0.2942 which signifies that the maximum variation of R_z from the means value is equal to 0.2942. The coefficient of determination (R) shows that the 98.1% outcome can be envisaged by the empirical model developed by this data due to controllable and non-controllable parameters. But adjusted R shows that 90.3% outcome can be envisaged by controllable factors only. Therefore, the value of adjusted R is always less than the R. As R_z is smaller, the better type quality attribute, so smaller value corresponding to the process parameter suggests its best level for minimum R_z. The results obtained (ranks of the input parameters) from Table 6 are in lined with ANOVA.

The surface quality largely depends upon the size of craters formed by debris erosion during machining. The erosion of material or debris is the result of thermal energy developed by discharge energy of the combination of input process parameters. Figure 8 presents the variation of important surface roughness parameter mean roughness depth R_z with respect to the input process parameters (i.e., SV, P_{on}, P_{off}, and WF) of wire-EDM in the present research. It can be observed from Fig. 8 that SV, WF, and P_{on} have the negative effect on surface quality of SMA. This happens due to the high thermal energy in the circuit whose main source is the discharge energy [17, 18].

It has been observed that the surface quality is deteriorating with the growth of spark gap set voltage. This happens due to the ionization of deionized water by which the discharge energy increases, and that causes increment in thermal energy. It overall results in formation of large and deeper craters on the machined surface. This makes the machined surface rough, i.e., increases R_z. In other words, the high surface irregularities occurred due to non-uniform crater formation after the effect of high thermal energy and deteriorate the machined surface.

Table 5 ANOVA for means (R_z)

Source	DF	SS	p (%)	MS	F value	P value
SV	3	2.670	19.98	0.890	10.29	0.044
P_{on}	3	4.884	36.54	1.628	18.81	0.019
P_{off}	3	3.068	22.96	1.022	11.82	0.036
WF	3	2.483	18.58	0.827	9.56	0.048
Residual error	3	0.259	1.94	0.086		
Total	15	13.364				

$S = 0.2942$; $R = 98.1\%$; adjusted $R = 90.3\%$

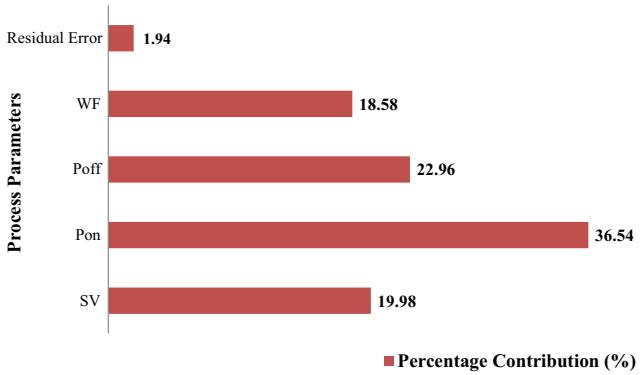

Fig. 7 Percentage contribution of each parameter for R_z

Table 6 Response table for means

Level	SV	P_{on}	P_{off}	WF
1	6.918	6.811	7.825	7.066
2	7.463	7.314	7.724	7.139
3	7.519	7.503	7.684	7.821
4	8.072	8.344	6.740	7.946
Delta	1.154	1.533	1.085	0.880
Rank	2	1	3	4

As shown in Fig. 8, high values of P_{on} also making the machined surface rough, as P_{on} is the main source of discharge energy as per Eq. (4). Low P_{on} values govern good surface morphology and hence the low roughness R_z, because the thermal energy generated due to discharge results in shallow and small craters.

Figure 8 depicts that surface roughness decreases with increase in P_{off}. Increasing P_{off} minimizes the spark intensity that results in low discharge and thermal energy, and hence, small shallower craters are formed that improves the surface conditions.

Good surface quality with lower roughness R_z has been observed with low wire feed rate WF. Because availability of fresh wire (having good cutting ability) at high feed rates increases the occurrence of spark and spark intensity, and thereby thermal energy which prompts, bigger crater formation, high amount of material removal, and surface deterioration.

Figure 9 illustrates the collective effect of P_{on} and P_{off} on R_z using contour plot. The color coding designated a range of R_z values. The best surface finish can be predicted from the values less than 6.5 μm. This R_z can be obtained at three conditions viz. P_{on} 0.35 μs and P_{off} 9 μs, P_{on} 0.35 μs and P_{off} 24 μs, and P_{on} 0.72 to 0.85 μs and P_{off} 22 to 24 μs. By this way, only projecting a point on contour graph and checking the corresponding color reveals the values of Rz along the combination of process parameters. Similarly, the contour plot has been obtained for R_z corresponding to P_{on} and SV (Fig. 10). The interactive relationship in between the P_{on} and SV has been studied considering R_z as a response variable. For every range of R_z, there are number of ranges of P_{on} and SV.

4 Modeling and optimization

As given in Eqs. (5) and (6), empirical models based on regression analysis have been developed to establish the relationship between wire-EDM parameters and responses.

$$\mathrm{MRR} = \varnothing\left(\mathrm{SV}, P_{on}, P_{off}, \mathrm{WF}\right) \tag{5}$$

$$Rz = \rho\left(\mathrm{SV}, P_{on}, P_{off}, \mathrm{WF}\right) \tag{6}$$

Various researchers have used regression analysis for modeling of machining processes [19, 20]. The main challenge is the prediction of regression coefficient using regression analysis.

Equations (7) and (8) are the regression equations developed for MRR and R_z.

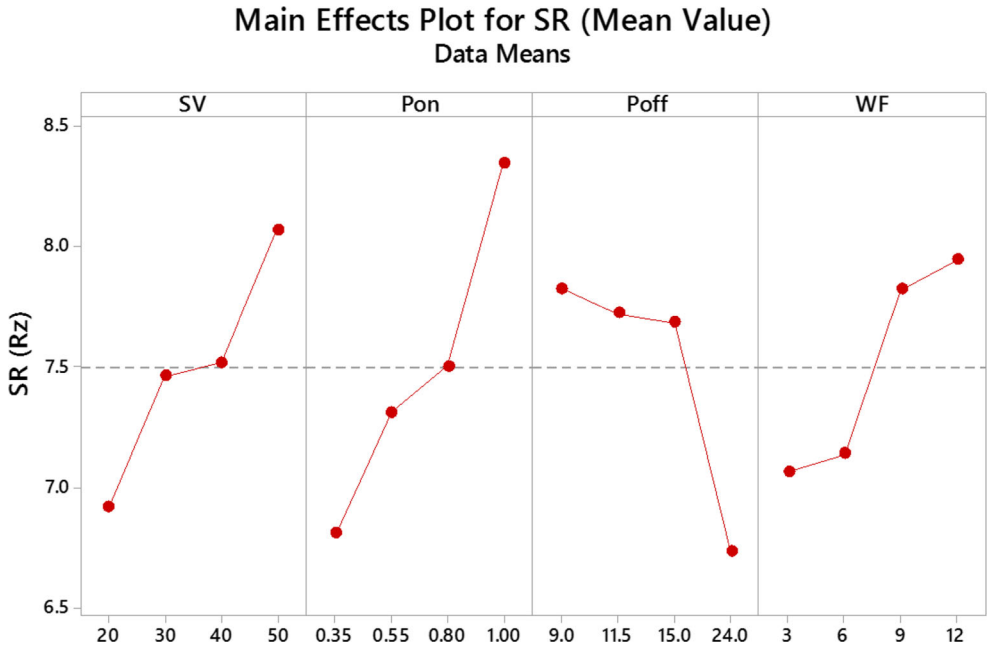

Fig. 8 Variation of R_z with wire-EDM parameters

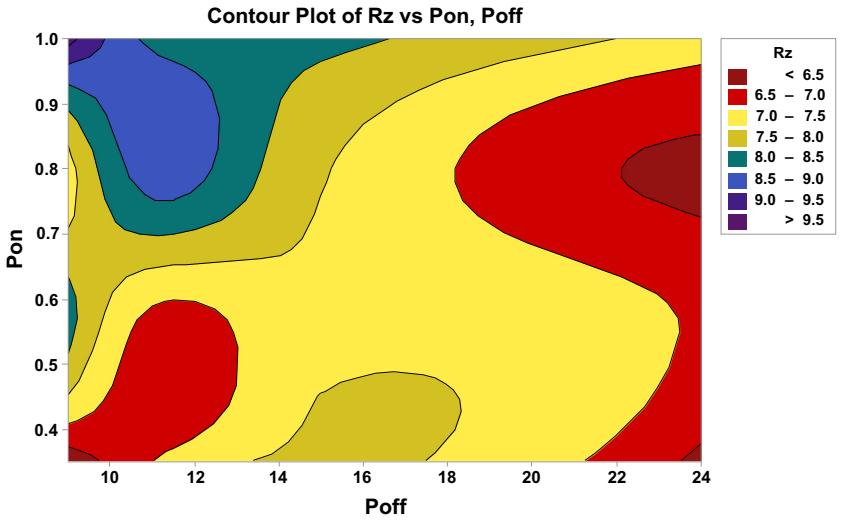

Fig. 9 Contour plot of R_z with P_{on} and P_{off}

$$\text{MRR} = -0.0033 + 0.0002\ \text{SV} + 0.0346\ P_{on} - 0.0005\ P_{off} + 0.0006\ \text{WF} \quad (7)$$

$$R_z = 5.08 + 0.035\ \text{SV} + 2.15\ P_{on} - 0.074\ P_{off} + 0.111\ \text{WF} \quad (8)$$

The residual plots for MRR and R_z have also been obtained. Figure 11 depicts the residual plots for MRR which includes normality, fitted versus predicted, histogram, and time-variance analysis. These analyses are mandatory for the verification of good ANOVA. The first test is the normality test in which all the residuals are laying on straight line as shown in Fig. 11. So, this verifies that there is no clustering of residuals and these are normally distributed. In residual versus fitted plot, it is found that all the residuals are randomly allocated, which claims a good statistical analysis by ANOVA. The parabolic structure is considered as the best solution for residual and ANOVA. So, the histogram test in the present work signifies satisfactory results of ANOVA. The time-variance plot in the ANOVA test does not represent any erratic change in the graph. This is mandatory for a significant ANOVA. Therefore, the entire four tests confirm the suitability of results of ANOVA for future outcome. Similarly, residual plot obtained in case of R_z (Fig. 12) verifies ANOVA results and their testing.

The development of non-dominated sorting algorithm (NSGA) was made my Srinivas and Deb [21] using ranking and non-dominating sorting procedure to solve a problem and attempts them to keep in the populations. NSGA has problems in selecting the optimal parameter from the sharing parameters, deficiency of elitism, and computationally complex. NSGA-II is the modified version of NSGA developed by Deb et al. [22] to overcome the drawbacks of NSGA. So, NSGA-II is computationally efficient, fast, non-elitism

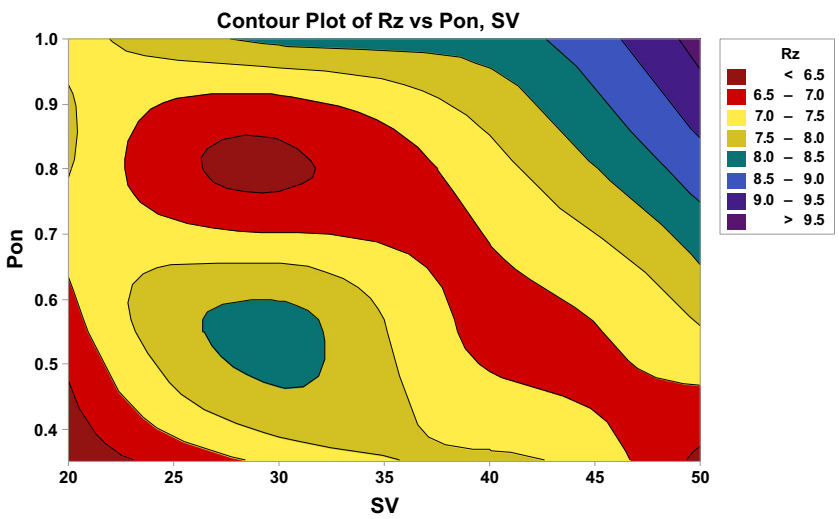

Fig. 10 Contour plot of R_z with P_{on} and SV

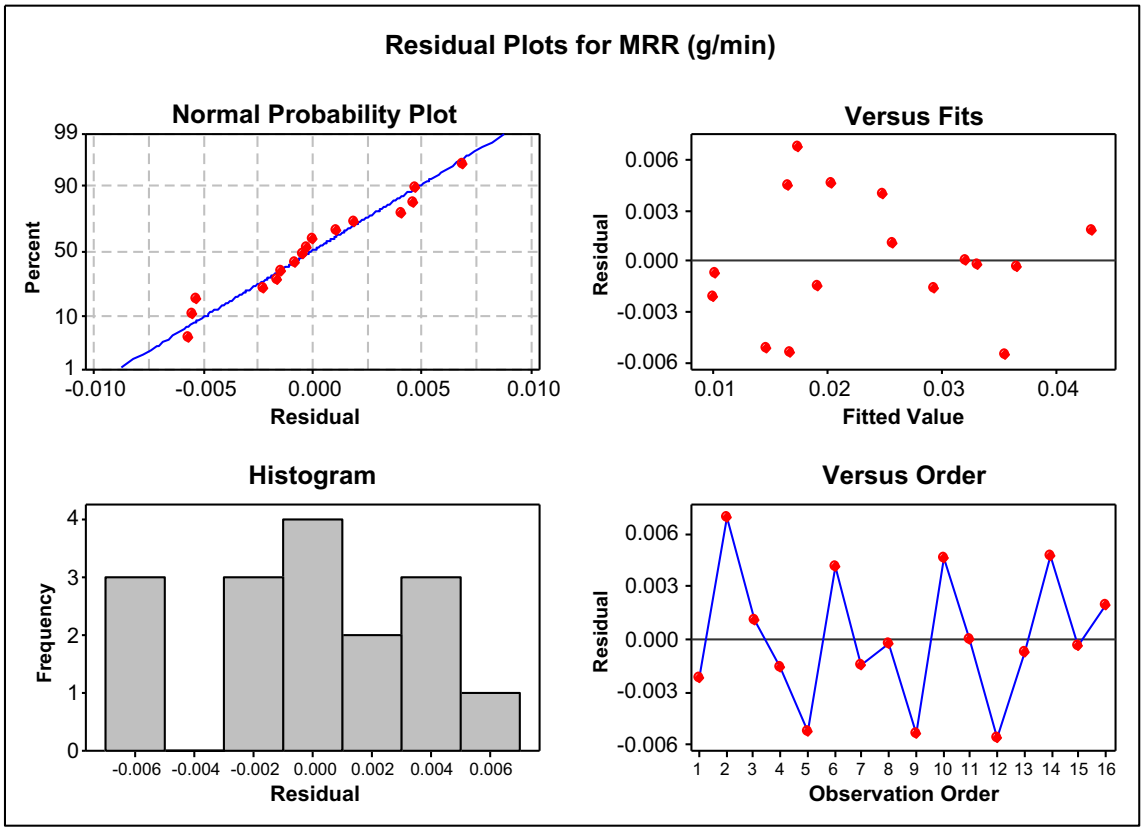

Fig. 11 Residual graph for MRR using regression analysis

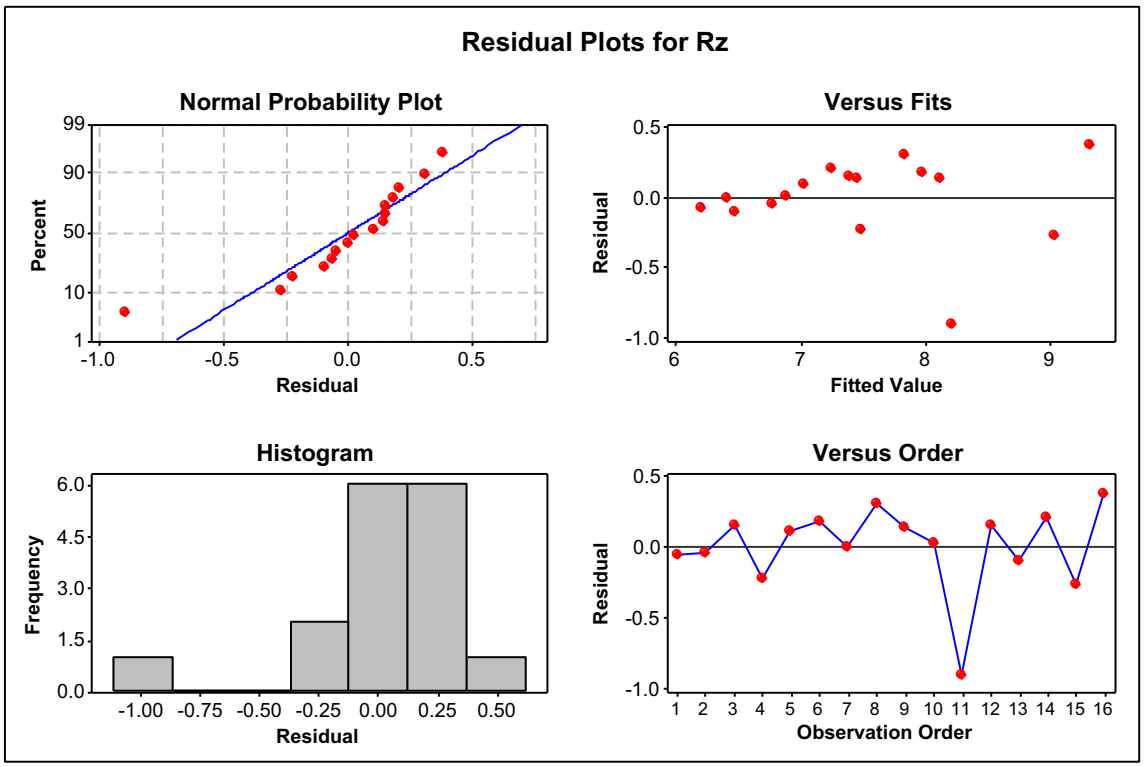

Fig. 12 Residual graph for R_z using regression analysis

preventing, non-dominating sorting, and less governed on sharing parameters to keep its diversity preservation. In the present work, two response variables viz. MRR and R_z have been investigated. These two responses are contradictory in nature. MRR has higher the better type attribute, while R_z has smaller the required type attribute. So, to predict the solutions by NSGA-II, the objective 1 (MRR) is modified according to negative for minimization. The objectives in the present work are given in Eqs. (9) and (10).

$$\text{Objective } 1 = -(\text{MRR}) \tag{9}$$

$$\text{Objective } 2 = (\text{SR}) \tag{10}$$

The operator considered for the present work is given in Table 7. The procedure of NSGA-II is described in the flow chart (Fig. 13). The steps describing the detailed method of NSGA-II is summarized in the below paragraphs.

Step 1. Population initialization

The population has been initialized based on the population range and the constraints.

Step 2. Non-dominating sorting procedure

After the initialization of the population as per the step (1), it is sorted by domination. It is critical during non-domination that one member exhibits better characteristics than the other.

(a) Solution p in population "P" can be obtained by following points,

(i) First point in this is the investigation of domination count (a_p). This a_p leads the p and is equal to the number of solutions.
(ii) Identify the set of solutions (S_s) from point (i). Also find S_s which represents a value greater than p.
(iii) Now for each individual r in population P

- If solution p dominates the individual r, then addition of S_s with r takes place; else if p does not lead r, then new $a_p = (a_{p+1})$.
- If $a_p = 0$, i.e., no solution dominates p, so p becomes first front "F1." Now give rank 1 to this p. The new F1 becomes (F1 + p).

(b) All individuals were solved as per the point "a" in the population P.
(c) Reduce the denomination counts of r from S_s by 1 for solution p with $a_p = 0$. After this, if still $a_p = 0$ for any member, place this in a separate list Q. The member in the list Q will belongs to the second front F2 (non-dominated).
(d) The points "a" to "c" are repeated till all the fronts in the population have been defined.

Step 3. Crowding distance

The crowding distance can be investigated depending upon the density of solutions adjacent to a solution in population. This requires categorization of the population as per the objective function in an increasing order (magnitude) for each front. The infinite distance values are allocated to the highest and smallest function values. The intermediate solutions have been assigned a normalized distance value, which is equal to the variance of two contiguous solutions. Now the crowding distance becomes equal to the summation of all distance values for each objective. This evolutionary algorithm does not need any type of user-defined factor for keeping the diversity in the population.

Step 4. Selection

Each individual in the population depicts two type of quality characteristics viz. crowding distance (k_{distance}) and non-dominated rank (k_{rank}). The following relation was kept in mind during the selection of any individual.

$$(k_{\text{rank}} < l_{\text{rank}}) \; or \; (k_{\text{rank}} = l_{\text{rank}}) \; and \; (k_{distance} > l_{distance})$$

The solution suggested in this way will reveal better rank with great diversity.

Table 7 Operators selection during NSGA-II

Operator	Type	Value
Crossover	Simulated binary	0.9
Selection	Non-dominating sorting and crowding distance	–
Mutation	Polynomial	0.1666
Generation	–	100
Population	–	500
Time taken		402 s (Average of 10)

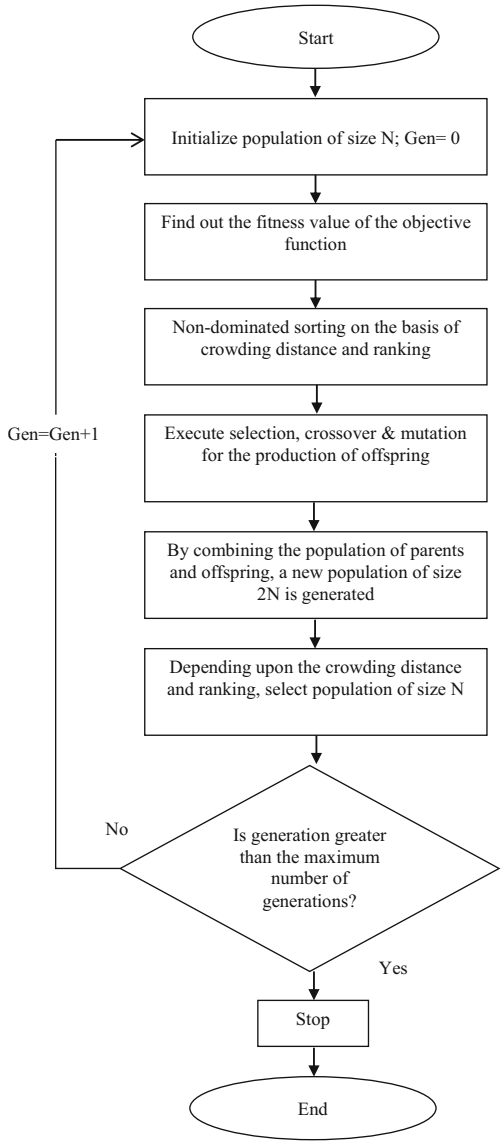

Fig. 13 NSGA-II flow chart

Step 5. Genetic operators

Reproduction is made according to simulate binary crossover (SBX). The working principle of SBX is single-point crossover on binary string. It will create two offspring by two parent solutions.

Step 6. Recombination and selection

The current generation population is combined with the offspring for the next generation. The elitism was ensured due to the involvement of current and previous population. This will run lasts till population size increases from current population.

The empirical models obtained from Eqs. (7) and (8) were incorporated in the objective functions of Eqs. (9) and (10). The upper and lower limits of process parameters (SV, P_{on}, P_{off}, and WF) were given in Eqs. (11), (12), (13) and (14).

$$20 \leq \mathrm{SV} \leq 50 \tag{11}$$

$$0.35 \leq P_{on} \leq 1 \tag{12}$$

$$9 \leq P_{off} \leq 24 \tag{13}$$

$$3 \leq \mathrm{WF} \leq 12 \tag{14}$$

There are two methods to check the computation effort (i) by using stop watch (ii) in-built commands of "tic" and toc at the starting and end of function. So, the mean elapsed time for 10 computations is 122 s (population 300, generation 80). The computation is also made for increasing the population (500) and generation (100) with a mean elapsed time of 402 s. So, with increasing the population and generation, the computational efforts become complex.

The Pareto optimal solution front is shown in Fig. 14. The X and Y axes in Pareto optimal front represent the SR (i.e., mean roughness depth) and MRR, respectively. It is clear from Fig. 14 that with the change of one response, the other response is also changed. It is obvious that the increase in MRR will deteriorate the surface characteristics of shape memory alloy. The predicted solutions suggested by NSGA-II are given in Table 8. These solutions have not been arranged on the basis of their superiority. Every suggested solution gives a value of MRR and R_z corresponding to the process parameters. Therefore, it is up to the operator or technician to select the responses (MRR and R_z) first, and according to the selected response, they will select the process parameters setting. NSGA-II provides a number of solutions, and according to the requirement of any industry, they will select the combination. So, to verify the results obtained from NSGA-II, five confirmatory experiments were performed on random basis (experiment numbers 1, 9, 17, 23, and 27). The suggested parametric settings given in Table 8 are in decimals. So, due to machine tool limitation, the nearby possible value was set for validation. It was found from the validation run that the MRR and R_z values are close to the predicted solutions (see Table 9), which claims successful process optimization by evolutionary algorithm NSGA-II.

The morphology of machined surface has also been studied at different combinations of parameter settings that generate different discharge energy. At low discharge energy level (Fig. 15a), the formation of deposited layer, surface cracks, and micro-pores is less as compared to high discharge energy level (Fig. 15b). The reason as discussed is the fast heating and cooling at high discharge

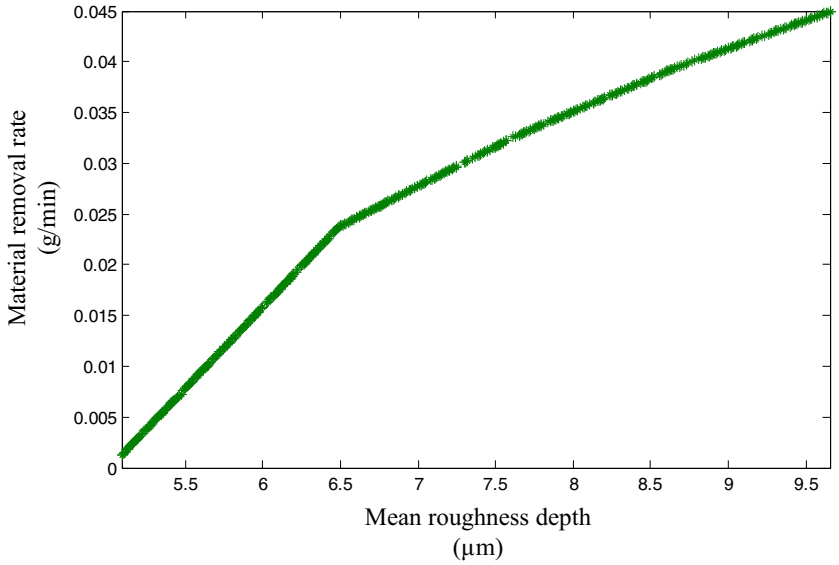

Fig. 14 Pareto optimal solution for 100 generations

Table 8 Predicted solutions suggested by NSGA-II

Sr. no.	SV	P_{on}	P_{off}	WF	MRR	R_z
1	50.00	1.00	9.00	12.00	0.045	9.65
2	20.00	0.35	24.00	3.00	0.001	5.09
3	20.00	0.35	24.00	3.00	0.001	5.09
4	50.00	1.00	9.00	12.00	0.045	9.65
5	20.00	0.41	24.00	3.00	0.003	5.23
6	20.00	1.00	12.98	3.00	0.030	7.30
7	20.04	1.00	12.45	3.00	0.030	7.34
8	20.00	0.40	24.00	3.00	0.003	5.20
9	20.03	0.89	24.00	3.05	0.020	6.27
10	49.43	1.00	9.00	6.20	0.041	8.99
11	27.34	1.00	9.00	3.00	0.034	7.85
12	27.87	1.00	9.00	3.12	0.034	7.89
13	20.00	0.88	24.00	3.00	0.019	6.24
14	31.43	1.00	9.09	3.00	0.035	7.99
15	29.12	1.00	9.03	3.00	0.034	7.91
16	49.23	1.00	9.00	9.68	0.043	9.37
17	25.37	1.00	9.21	3.00	0.033	7.77
18	20.00	0.56	24.00	3.00	0.008	5.54
19	20.00	0.56	24.00	3.00	0.008	5.56
20	29.70	1.00	9.00	3.00	0.034	7.94
21	20.04	1.00	19.41	3.01	0.026	6.83
22	20.00	0.49	23.95	3.00	0.006	5.41
23	20.37	1.00	19.96	3.00	0.026	6.80
24	26.15	1.00	9.20	3.00	0.033	7.80
25	20.00	0.61	24.00	3.00	0.010	5.65
26	20.11	1.00	20.92	3.00	0.025	6.72
27	48.44	1.00	9.00	6.06	0.040	8.94
28	49.62	1.00	9.00	6.54	0.041	9.03
29	20.00	0.59	24.00	3.00	0.009	5.62
30	20.00	0.60	24.00	3.00	0.010	5.63

energy level. The temperature in the circuit becomes very high due to the thermal energy induced at high discharge parameters as compared to the temperature obtained at low discharge parameters. At high temperature, material started to melt and evaporate and eventually came to the contact of dielectric. This dielectric reduced the temperature and quenched the material. Due to this quenching effect, the deposited layer, surface cracks, and sub-surface have appeared. Moreover, the excessive material removal made the debris particles to stick in the machining zone in the absence of proper flushing and that redeposited on the machined surface.

But, at low discharge parameter combinations, the quenching effect and material deposition are not as severe as in high discharge parameters. The surface morphology of the suggested (NSGA-II) solutions has also been investigated. Figure 15c, d shows the SEM micrograph at predicted solution 1 and predicted solution 9, respectively. The presence of micro-pores, micro-crack, lumps, and deposited layer is found. At every setting of the process parameters, there is some discharge energy level, so the formation of micro-pores, lumps, deposited layer, and sub-surface cannot be eliminated completely. But process parameter optimization can significantly reduce the surface morphology deterioration at a great extent as observed and discussed in the present research work.

5 Conclusions

In the present paper, the important results of the investigation on wire-EDM of $Ni_{55.8}Ti$ shape memory alloy are reported and discussed. The following conclusions can be drawn from this work:

Table 9 Validation runs on predicted solutions

Sr. no.	SV	P_{on}	P_{off}	WF	Predicted		Experimental		Error (%)	
					MRR	R_z	MRR	R_z	MRR	R_z
1	50	1	9	12	0.045	9.65	0.044	9.52	2.44	1.4
9	20	0.9	24	3	0.020	6.27	0.021	6.20	−4.95	1.16
17	25	1	9	3	0.033	7.77	0.033	7.53	2.38	3.15
23	20	1	20	3	0.026	6.80	0.027	7.15	−3.43	−5.08
27	48	1	9	6	0.040	8.94	0.042	9.26	−3.17	−3.56

- Wire-EDM of $Ni_{55.8}Ti$ at higher voltage, pulse-on time, and wire feed rate resulted in higher material removal rate, i.e., high productivity.
- High discharge energy parameter settings deteriorated the surface quality with high occurrence of cracks, deposited layers, and lumps, and generated rough surfaces on the machined $Ni_{55.8}Ti$ samples.
- The developed empirical models accurately predict the MRR and R_z values.
- NSGA-II successfully envisage the solution, i.e., process parameters corresponding to different MRR and R_z.

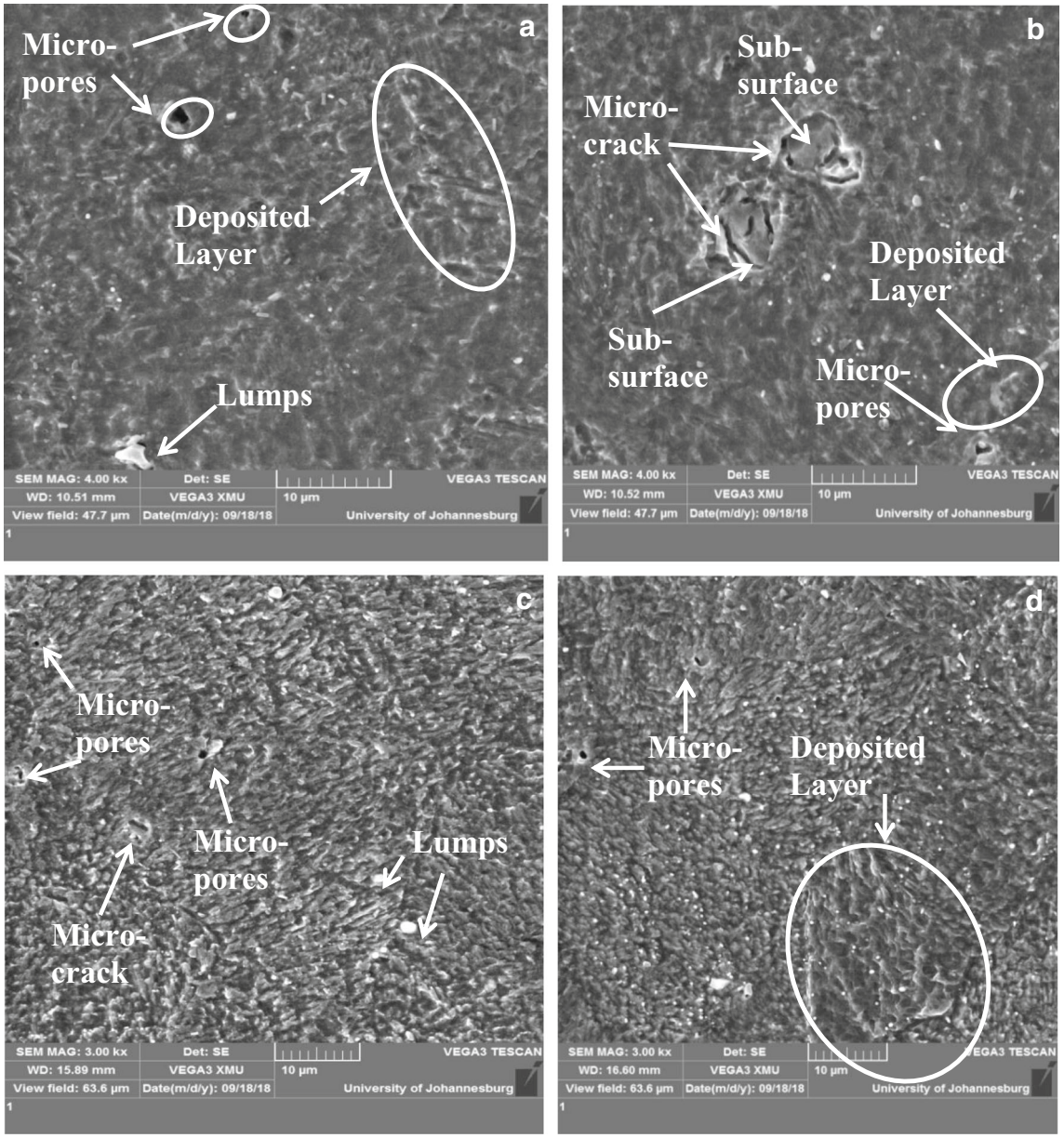

Fig. 15 SEM micrographs of SMA samples machined by wire-EDM at **a** low discharge energy: experiment 1, **b** high discharge energy: experiment 16, **c** validation run of predicted solution 1, and **d** validation run of predicted solution 9

- Wire-EDM of $Ni_{55.8}Ti$ at parameters optimized by NSGA-II resulted in improved surface quality (R_z—6.20 μm) and process productivity (MRR—0.021 g/min) at a single set. Based upon the requirements, the NSGA solutions as obtained in the present work can be referred for better process performance.

Acknowledgements This research work is supported by URC 2018/19 grant of University of Johannesburg.

References

1. Jani JM, Leary M, Subic A, Gibson MA (2014) A review of shape memory alloy research, applications and opportunities. Mater Des 56:1078–1113
2. Markopoulos AP, Pressas IS, Manolakos DE (2016) Chapter 7 Manufacturing Processes of Shape Memory Alloys in JP Davim Eds, Materials Forming and Machining, Elsevier, 155–180
3. Mehta K, Gupta K (2019) Fabrication and processing of shape memory alloys. Springer- Switzerland
4. Yokoyama K, Hamada K, Moriyama K, Asaoka K (2001) Degradation and fracture of Ni-Ti superelastic wire in an oral cavity. Biomaterials 22:2257–2262
5. Guo Y, Klink A, Fu C, Snyder J (2013) Machinability and surface integrity of nitinol shape memory alloy. CIRP Ann 62:83–86
6. Gao S, Huang H (2017) Recent advances in micro- and nano-machining technologies. Front Mech Eng 12:18–32
7. Rajurkar KP, Sundaram MM, Malshe AP (2013) Review of electrochemical and electrodischarge machining. Procedia CIRP 6:13–26
8. Gupta K, Jain NK (2016) Chapter-2 "Overview of wire spark erosion machining", In Near Net Shape Manufacturing of Miniature Spur Gears, Springer
9. Manjaiah M, Laubscher RF, Narendranath S, Basavarajappa S, Gaitonde VN (2016) Evaluation of wire electro discharge machining characteristics of Ti50Ni50-xCux shape memory alloys. J Mater Res 31:1801–1808
10. Manjaiah M, Narendranath S, Basavarajappa S, Gaitonde VN (2015) Effect of electrode material in wire electro discharge machining characteristics of Ti50Ni50-xCux shape memory alloy. Precis Eng 41:68–77
11. Sharma N, Raj T, Jangra KK (2017) Parameter optimization and experimental study on wire electrical discharge machining of porous Ni40Ti60 alloy. Proc IMechE Part B: J Eng Manuf 231:956–970. https://doi.org/10.1177/0954405415577710
12. Soni H, Narendranath S, Rangarasaiah RM (2017) An experimental study of influence of wire electro discharge machining parameters on surface integrity of TiNiCo shape memory alloy. J Mater Res 32:3100–3108
13. Bisaria H, Shandilya P (2018) The machining characteristics and surface integrity of Ni-rich NiTi shape memory alloy using wire electric discharge. Proc IMechE Part C: J Mech Eng. https://doi.org/10.1177/0954406218763447
14. Bhushan B (2013) Introduction to tribology. Wiley and Sons, New York
15. Petropoulos GP, Pandazaras CN, Davim JP (2010) Surface texture characterization and evaluation related to machining. In: Surface integrity in machining. Springer, London, pp 37–66
16. Montgomery DC (2009) Design and analysis of experiments, 7th edn. John Willey & Sons, New Delhi
17. Tonday HR, Tigga AM (2016) Analysis of effects of cutting parameters of wire electrical discharge machining on material removal rate and surface integrity. IOP Conf Ser: Mater Sci Eng 115:012013
18. Mouralova K, Kovar J, Klakurkova L, Prokes T, Horynova H (2017) Comparison of morphology and topography of surfaces of WEDM machined structural materials. Measurement 104:12–20
19. Mouralova K, Matousek R, Kovar J, Mach J, Klakurkova L, Bednar J (2016) Analyzing the surface layer after WEDM depending on the parameters of a machine for the 16MnCr5 steel. Measurement 94:771–779
20. Sahoo AK, Pradhan S (2013) Modeling and optimization of Al/SiCpMMC machining using Taguchi approach. Measurement 46:3064–3072
21. Srinivas N, Deb K (1994) Multi objective optimization using non-dominated sorting algorithm. Evol Comput 2:241–248
22. Deb K, Pratap A, Agarwal S, Meyarivan T (2002) A fast and elitist multi-objective genetic algorithm: NSGA-II. IEEE T Evolut Comput 6:182–197